Systematic Approach to Understanding Macrolide−Ribosome Interactions: NMR and Modeling Studies of Oleandomycin and Its Derivatives†

Predrag Novak,*,‡,§ Iva Tatić,*,§ Predrag Tepeš,§ Sanja Koštrun,§ and Jill Barber||

Faculty of Natural Sciences, Department of Analytical Chemistry, University of Zagreb, Horvatovac 102a, HR-10000 Zagreb, Croatia, PLIVA-Research Institute Ltd, Prilaz baruna Filipovića 29, HR-10000 Zagreb, Croatia, and School of Pharmacy and Pharmaceutical Sciences, University of Manchester, Manchester, U.K. M13 9PL

Received: May 19, 2005; In Final Form: June 30, 2005

The three-dimensional structures of oleandomycin (**1**) and its derivatives oleandomycin-9-oxime (**2**) and 10,11-anhydrooleandomycin (**3**) were determined in different solvents by the combined use of NMR and molecular modeling methods. The experimental NMR data were compared with the results of molecular modeling and known crystal structures of the related molecules. It was shown that the dominant conformation of the lactone ring is the folded-out conformation with some amounts of the folded-in one depending on the solvent and temperature, while desosamine and cladinose sugars adopt the usual chair conformations. Modeling calculations provided evidence for conformational changes in the upper lactone region as well. Saturation transfer difference (STD) NMR experiments have provided information on the binding epitopes of **1**−**3** in complexes with *E. coli* ribosomes. The obtained molecular surfaces in close contact with ribosomes were compared with recently available 3D structures of the related macrolide−ribosome complexes, and the observed differences were discussed. The knowledge gained from this study can serve as a platform for the design of novel macrolides with an improved biological profile.

Introduction

Macrolide antibiotics are therapeutically important agents that are effective inhibitors of bacterial protein biosynthesis. They bind to the large 50S ribosomal subunit at or near the peptidyl transferase center and block the elongation of the peptide chain.[1] Recently, structures of macrolide−ribosome complexes at atomic resolution have become available, providing information about the macrolide binding mode and about the major causes of resistance in bacteria.[2−4] The binding affinity is achieved by hydrophobic and hydrogen bonding interactions between ribosomes and macrolides.[3] Understanding the mechanism by which macrolides exert their activity is crucial for the design of novel molecules with an improved overall biological effect.

Oleandomycin (**1**) and its derivatives oleandomycin-9-oxime (**2**) and 10,11-anhydrooleandomycin (**3**) (Figure 1) consist of a 14-membered macrocycle ring and two cyclic sugars, oleandrose and desosamine.[5,6] Oleandomycin differs from erythromycin by the exocyclic epoxide at C8, being a unique feature without being equal in any other known polyoxo macrolide.

A variety of approaches to understanding the conformations of macrolides in solution have been employed over the years. All have involved a combination of NMR and modeling methods. The NMR data used include coupling constants, especially in the macrolide ring, and nuclear Overhauser effect (NOE) data.[7−15] Here, conventional nuclear Overhauser enhancement spectroscopy (NOESY) experiments are subject to errors because macrolide NOEs are close to zero at commonly used field strengths. The rotating frame experiments (ROESY) give rise to equally weighted positive signals but are technically demanding and very susceptible to artifacts. In some studies, NMR constraints were applied in molecular modeling calculations;[8−10] in others, molecular modeling calculations were carried out unconstrained and the resulting conformations compared with the NMR data.[7,11] The problem with applying constraints in the calculations is that average conformations that do not actually exist may be obtained. Such artificial conformations will have higher energies than the conformations obtained from unconstrained calculations, so it is possible to obtain satisfactory results using this approach by comparing the energies of the most favored structures with those from calculations without constraints. It is clear, however, that the method is both less generally applicable and more time-consuming than comparing NMR data with structures from unconstrained minimizations.

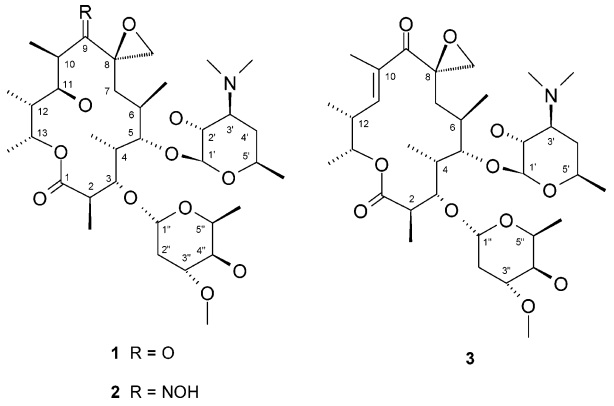

Figure 1. Compounds studied and the atom numbering.

† Part of the special issue "Donald G. Truhlar Festschrift".

* To whom correspondence should be addressed. E-mail: pnovak@chem.pmf.hr (P.N.); iva.tatic@pliva.hr (I.T.). Phone: 0038513721933. Fax: 0038513721570.

‡ University of Zagreb.

§ PLIVA-Research Institute Ltd.

|| University of Manchester.

10.1021/jp0526243 CCC: $33.50
Published on Web 08/06/2005

Accordingly, when we analyzed the conformation of oleandomycin-like compounds in solution, we used unconstrained molecular modeling calculations and then fitted the NMR data to the resulting structures.[7] Those results demonstrated that vicinal coupling constants (^3J(H2,H3)) and NOE proton−proton distances H3−H11 and H4−H11 can serve as good indicators of the aglycone ring folding. However, the 14-membered ring macrolides are highly constrained and therefore Steinmetz et al.,[8−10] for example, obtained results broadly in agreement with ours.

Many conformational analyses of erythromycin, azithromycin, and clarithromycin[9−15] have confirmed that macrolides exist in the two major conformational families: folded-out and folded-in, referring to the outward and inward folding of the ring fragment C3−C5. Our results on **1** and its 8-methylene-9-oxime derivative have shown that both conformational families exist in solution and that their ratio is dependent upon the temperature and the solvent used.[7]

This work is a continuation of our efforts to elucidate a three-dimensional structure of oleandomycin-like compounds and also describes attempts to correlate structures with biological activity. In particular, by determining conformations of **2** and **3**, we sought to establish whether structural differences in the upper lactone region have an impact on the overall conformation of the molecules. We then aimed to characterize interactions of **1**−**3** with ribosomes at the molecular level and to identify key structural parts responsible for activity. This information is valuable in the design of more potent molecules.

Two interactions (weak and strong) between macrolides and ribosomes have been demonstrated.[16−18] The weak binding seems to be the first step of recognition and selection of antibiotics by the ribosomal machinery. It is characterized by a fast chemical exchange rate and therefore is suitable for NMR experiments. Thus, we combine here transferred NOESY (trNOESY) and saturation transfer difference (STD) NMR experiments to probe bound macrolide conformations and to determine regions of the molecule in close contact with the ribosome. The STD method has been shown to be sensitive and reliable for determining the binding epitopes of ligand−receptor interactions in general.[19] It is based on a magnetization transfer by macromolecule signal saturation and its relayed effect to the ligand. Here, we use the STD method to study complexes between *E. coli* ribosomes and compounds **1**−**3**. The trNOESY experiment is widely used to gain structural information about bound drugs.

Experimental Section

NMR Measurements. NMR spectra were recorded at room temperature on a Bruker Avance DRX500 spectrometer with a 5 mm diameter QNI inverse detection probe and a *z*-gradient coil. Tetramethylsilane (TMS) was used as the internal standard. The concentration of the samples was 20 mg mL^{-1} in $CDCl_3$, acetone-d_6, and DMSO-d_6 solutions.

The proton spectra were recorded with a spectral width of 5500 Hz and a pulse width of 11.2 μs (90° flip angle). Thirty-two scans and a repetition rate of 6 s (2 s for the acquisition time and 4 s for the relaxation delay) were used. Processing, performed with exponential multiplication, was carried out with a 16K data table, giving the digital resolution of 0.16 Hz per point.

For recording carbon spectra, the APT pulse sequence within Bruker software was used. Data were collected with a spectral width of 32 000 Hz in a block of 64K and a pulse width of 8.9 μs (90° flip angle). Five thousand scans and a repetition rate of 3 s (1 s for the acquisition and 2 s for the relaxation delay) were used. Exponential weighting with a line broadening of 1 Hz was applied before Fourier transformation. The digital resolution was 0.96 Hz per point.

The ^{1}H−^{1}H shift correlated two-dimensional correlation spectroscopy (COSY) spectra were obtained using the double quantum filtered (DQF)-COSY pulse sequence. The COSY spectra were recorded under the following conditions: the spectral width was 5500 Hz in both dimensions, 2K data points were applied in the time domain and 1k increments were collected for each data set with linear prediction and zero filling to 2K. Eight scans were applied for each increment. The relaxation delay was 1 s. Spectra were processed with an unshifted sine function. The digital resolution was 2.2 Hz per point in both domains.

States-time-proportional phase incremation (TPPI) sensitive ROESY spectra were obtained using the experiment of Bax and Davis.[20] A mixing time of 250 ms was used, and spectra were processed with a sine squared function shifted by $\pi/2$ in both domains, giving a digital resolution of 2.2 Hz per point in both domains. The pulse length, the spectral width, and the initial and final matrices were used as in the COSY experiment.

The one-bond ^{1}H−^{13}C chemical shift heteronuclear single-quantum correlation (HSQC) experiment was obtained using the standard pulse sequence using B_0 gradient pulses for the selection of ^{1}H nuclei coupled to ^{13}C carbons. The conditions for recording HSQC experiments were the following: the relaxation delay was 2 s, and 32 scans per increment were executed. The spectral width was 5500 Hz in acquisition domain f2 and 21 000 Hz in time domain f1. Data were collected into a 2K × 256 acquisition matrix and processed using a 2K × 1K transformed matrix with zero filling in the f1 domain. Sine multiplication was performed before Fourier transformations, giving a final digital resolution of 7.33 Hz in f2 and 30.71 Hz in the f1 dimension.

The ^{1}H detected heteronuclear multiple bond correlation (HMBC) spectra were recorded using the pulse sequence proposed by Bax and Summers[21] involving a low-pass *J*-filter (3.4 s) and a delay for long-range coupling of 65 ms. The acquisition and processing parameters were the same as those used in the HSQC experiment.

The States-TPPI phase sensitive T-ROESY spectra were obtained using the experiment developed by Hwang and Shaka[22] that is designed to suppress the TOCSY/COSY cross-peaks. The experimental conditions were the same as those described above for the standard ROESY.

Sample Preparation. Ribosomes were isolated from the *E. coli* MRE 600 strain by the zonal ultracentrifuge technique. Fully deuterated ribosomes isolated from the *E. coli* MRE 600 strain were purchased from CDN Ltd. Leete Str. 13, 11313 Tallin, Estonia.

For trNOESY experiments, the compounds were dissolved in the aqueous 20 mM deuterated tris(hydroxymethyl)aminomethane (Tris) buffer with 60 mM KCl for better ribosomal stability at physiological apparent pH 7.4 and the concentration was 4 mM. For measuring the trNOESY spectra, the solution of **1**−**3** was titrated with ribosomes until a final concentration of 0.8 μM ribosome was achieved. The measurements were acquired with a total volume of 600 μL and a ribosome/macrolide ratio of 1/3000−1/4000, which is usual for the related molecules.[16−18]

STD Measurements. 1D STD NMR spectra were collected with 16k data points and a spectral width of 15 ppm by using a sequence provided by Bruker. Selective saturation of the *E.*

coli ribosomes was first performed using a 50 ms Gaussian and 50 ms E-BURP pulses. The two pulses gave similar STD results, but the E-BURP pulse was proven to be better, owing to its higher sensitivity and selectivity. The E-BURP pulse was then applied at varying duration and saturation time to reach the optimum experimental conditions. The saturation time was 2−4 s. The saturated and reference spectra were acquired and processed simultaneously by creating a pseudo-2D experiment. The saturation frequency was switched from on-resonance (−1 ppm) to off-resonance (35 ppm) after each scan. The WATERGATE[23,24] pulse train was used to suppress the HDO signal.

trNOESY Measurements. The trNOESY spectra were acquired using the pulse sequence for phase sensitive 2D homonuclear correlation (*noesygptp19*) provided by Bruker software. A data matrix of 2K × 512 complex points and 8 scans with a sweep width of 5000 Hz was used. The mixing time was 100−200 ms. Data were zero filled in f1 to 1K and transformed using a sine squared function, giving a digital resolution of 2.44 Hz in f2 and 4.88 Hz in the f1 dimension. The WATERGATE sequence[23,24] was used for the suppression of the HDO signal.

Molecular Modeling. All computational results were obtained using an SGI Origin 3400 platform running software programs InsightII, Builder, Discover, and Analysis, version 2000.1 (Molecular Simulations Inc.). Dynamics calculations were done with the Discover program, version 2000.1 (Molecular Simulations Inc.), using the cvff force field.

As a starting structure for molecular modeling calculations, the structure deposited at CSD[25] under the BBOLEA code[26] was used (the bromobenzoyl substituent was removed to obtain the 3D structure that corresponded to the 3D structure of oleandomycin). Additional modifications were also made to the same structure to obtain structures **2** and **3** (Figure 1) used for simulations. These were minimized using a combination of steepest descent and conjugate gradient algorithm.

Minimized structures were solvated in a 40 Å dimethyl sulfoxide (DMSO) box (provided by InsightII package) and $CDCl_3$ (provided by Accelrys). The solvents for simulations were chosen according to the effects of interest in the NMR data. The minimization and dynamics (15 ps) of the solvent were performed while keeping the solute fixed. Subsequently, the solute was kept unfixed and the system was gradually heated to 700 K and equilibrated for 20 ps. The elevated temperature was used to search the entire conformational space, at the acceptable length of simulation duration. The time step used was 1 fs. A 15 Å nonbonded cutoff was applied. The production phase of the simulation lasted 1 ns at 700 K, under NVT conditions. The temperature was kept constant by coupling to a heat bath using the Andersen algorithm. For analysis, trajectory and energy data were saved every 100 fs during the production phase. Computational results were obtained using software programs from Molecular Simulations Inc., and dynamics calculations were done with the Discover program, using the cvff force field.

Results and Discussion

Assignments of the NMR Spectra. The proton and carbon chemical shifts of **1**−**3** in all three solvents were assigned by the combined use of one- (^{1}H and APT) and two-dimensional NMR spectra (gDQF-COSY, gHSQC, and gHMBC). The APT pulse sequence was used to ascertain the hydrogen multiplicity of the carbon signals. The COSY spectra revealed all of the expected geminal and vicinal correlations characteristic of the structures depicted in Figure 1. The HSQC spectra yielded an unambiguous assignment for the protonated carbon atoms, while correlation peaks in HMBC spectra revealed information about the quaternary carbons and confirmed the assignments of the protonated carbons. The values obtained in $CDCl_3$ are in good agreement with those reported previously.[6] The chemical shifts obtained in acetone-d_6 and DMSO-d_6 (Table 1) are similar to those in $CDCl_3$. Homonuclear vicinal coupling constants were extracted from the high-resolution one-dimensional proton and two-dimensional DQF-COSY spectra and are listed in Table 2. Since the NOE of **1**−**3** at 11.7 T approaches zero, NOE data were obtained from the analysis of the two-dimensional ROESY or T-ROESY spectra and the one-dimensional selective ROESY experiments. Two-dimensional NOESY experiments were employed for the solution of **1**−**3** and the *E. coli* ribosomes.

TABLE 1: Proton and Carbon Chemical Shifts of 1−3 in DMSO-d_6

	1		**2**		**3**	
atom	^{1}H/ppm	^{13}C/ppm	^{1}H/ppm	^{13}C/ppm	^{1}H/ppm	^{13}C/ppm
1		175.37		174.07		173.75
2	2.61	43.12	2.69	43.87	2.54	44.34
2Me	1.07	11.95	1.08	14.48	1.10	14.37
3	3.70	77.67	3.57	79.82	3.52	79.68
4	1.73	43.84	1.59	41.37	1.68	41.89
4Me	1.06	8.84	1.10	8.77	1.06	9.50
5	3.33	81.57	3.35	82.88	3.27	84.23
6	1.87	31.38	2.09	28.02	1.65	30.59
6Me	1.05	18.03	0.97	17.70	1.01	16.70
7a	2.23	37.92	1.94	33.97	2.50	35.32
7b	1.37	37.92	1.22	33.97	1.15	35.32
8		62.91		82.81		61.19
8a	2.65	48.80	4.24	81.23	2.94	49.31
8b	2.65	48.80	3.70	81.23	2.74	49.31
9		206.40		163.09		198.26
10	3.03	44.35	2.58	33.06		135.44
10Me	0.88	8.62	1.05	7.68	1.77	11.40
11	3.66	68.99	3.75	68.17	6.64	143.25
12	1.56	39.77	1.59	40.61	3.16	35.25
12Me	0.86	7.50	0.84	8.45	0.97	14.70
13	5.19	69.35	5.50	69.08	4.83	74.15
13Me	1.20	17.20	1.18	18.24	1.28	13.22
1′	4.08	103.42	4.10	103.67	4.10	104.59
2′	3.06	69.69	3.04	69.66	3.04	70.21
3′	2.45	64.12	2.47	64.01	2.46	64.58
3′NMe$_2$	2.21	55.94	2.20	39.72	2.20	40.34
4′a	1.62	29.39	1.61	29.30	1.16	29.86
4′b	1.13	29.39	1.12	29.30	1.12	29.86
5′	3.42	67.72	3.41	67.57	3.41	68.18
5′Me	1.14	20.53	1.11	20.54	1.10	20.99
1″	4.79	97.81	4.84	98.59	4.61	89.81
2″a	2.23	33.89	2.21	33.97	2.15	34.12
2″b	1.35	33.89	1.40	33.97	1.39	34.12
3″	3.28	77.05	3.27	76.85	3.22	77.119
3″OMe	2.32	55.98	3.33	56.17	3.31	56.58
4″	2.88	74.95	2.84	75.13	2.78	75.71
5″	3.53	68.51	3.57	68.48	3.38	68.98
5″Me	1.11	17.25	1.18	17.24	1.10	17.38

Conformations of the Macrocycle Ring. It is now well established that the macrocyclic ring adopts two major types of conformations in the C3 to C5 region; these are known as folded-in and folded-out.[7,12−14] The folded-in conformational family is characterized by a close approach of H3 to H11 and of H4 to H6Me. The vicinal H2−H3 scalar coupling constant (^3J(H2,H3)) is approximately 2−3 Hz. The folded-out conformational family is characterized by a close approach of H4 to H11 and a higher ^3J(H2,H3) value of up to 10 Hz.

We have previously shown[7] that **1** exists predominantly in the folded-in conformation in DMSO-d_6 but adopts a mixture of folded-in and folded-out conformations in D_2O, acetone-d_6, and $CDCl_3$. We also observed that for **1** and its 8-methylene-

TABLE 2: Vicinal Proton−Proton Coupling Constants (*J*, Hz) for 2 and 3 in Different Solvents

	J					
	2			**3**		
atoms	DMSO-d_6	acetone-d_6	$CDCl_3$	DMSO-d_6	acetone-d_6	$CDCl_3$
2H−3H	9.2	9.3	9.6	6.7	5.8	4.8
3H−4H	*a*	1.1	1.1	1.3	1.8	1.8
4H−5H	10.5	10.9	10.5	10.3	10.0	9.9
5H−6H	1.8	*b*	1.5	*a*	*a*	1.2
6H−7aH	1.0	2.4	1.2	*a*	3.1	3.1
6H−7bH	11.1	10.9	11.3	*b*	*b*	7.9
10H−11H	1.6	2.0	2.1			
10MeH−11H				1.5	1.5	1.4
11H−12H	10.3	10.2	10.4	10.3	10.2	9.9
12H−13H	*a*	1.0	1.0	4.7	4.8	4.8
1′H−2′H	7.3	7.3	7.3	7.3	7.3	7.3
2′H−3′H	9.9	10.2	10.2	10.0	10.2	10.3
3′H−4aH	4.0	3.9	3.9	4.1	4.0	3.9
3′H−4′bH	*b*	12.4	12.2	10.2	10.2	10.3
4′aH−5′H	1.7	2.2	2.1	1.8	2.1	2.1
4′bH−5′H	11.1	10.9	10.7	10.7	10.8	10.8
1″H−2″aH	1.3	1.3	1.2	1.3	1.4	1.3
1″H−2″bH	4.1	3.8	3.9	3.7	3.7	3.7
2″aH−3″H	4.6	4.7	4.6	4.8	4.6	4.5
2″bH−3″H	11.6	11.6	11.6	11.7	11.7	11.7
3″H−4″H	8.8	9.0	8.9	8.4	9.1	9.0
4″H−5″H	9.1	9.3	9.4	9.2	9.3	9.2

[a] Unresolved. [b] Signal Overlap.

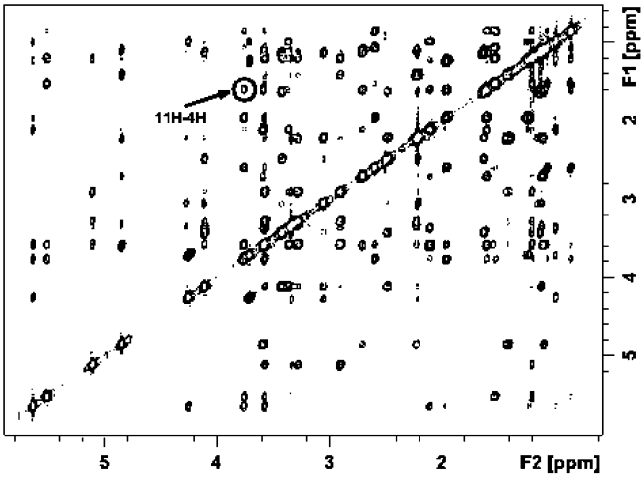

Figure 2. Two-dimensional ROESY spectrum of **2** in DMSO-d_6.

9-oxime derivative ^3J(H2,H3) was the only coupling constant affected by changing the temperature and the solvent polarity; other changes were not significant.[7]

2 behaves rather differently. In DMSO-d_6, acetone-d_6, and $CDCl_3$, ^3J(H2,H3) is around 9 Hz, suggesting that **2** exists mainly in the folded-out form. The presence of H4−H11 NOE cross-peaks (Figure 2) and the absence of H3−H11 cross-peaks provides further evidence for this conclusion. The molecular dynamics simulations, however, indicate that a small proportion of the folded-in conformational family may exist in DMSO and chloroform.

Table 2 shows that compound **3** behaves in a manner intermediate between **1** and **2**. ^3J(H2,H3) varies between 4.8 and 6.7 Hz at room temperature and is the highest in nonpolar $CDCl_3$. In **1**, the reverse is the case.[7] The conjugated ene−one system in **3** would be expected to have a profound effect on the conformational flexibility of the macrocycle, especially but not solely in the upper part of the ring. This is particularly true as the ene−one in **3** replaces the 9-ketone and OH group in **1**;

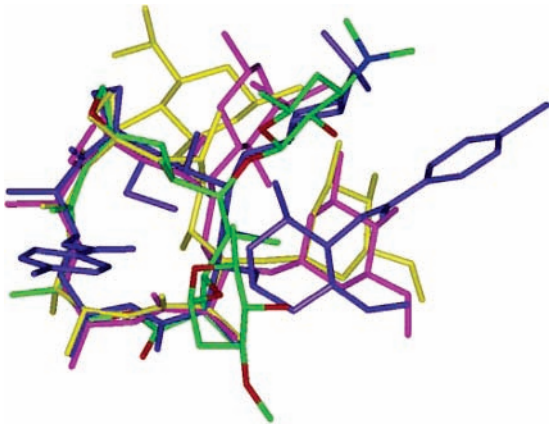

Figure 3. Superposition of the folded-in (by atom) and folded-out (yellow) conformations of **3** as determined by MD simulations and crystal structures of BOLEA (magenta) and ZATPAL (blue), representative of the folded-in and folded-out conformations, respectively, for oleandomycin-like compounds.

TABLE 3: Temperature Effects on ^3J(H2,H3) (Hz) in DMSO-d_6 for Compounds 1−3

	^3J(H2,H3)		
temperature/°C	**1**[a]	**2**	**3**
27	3.8	9.2	6.7
50	4.0	8.7	6.6
80	4.5	8.3	6.6
100	4.7	7.8	6.7

[a] Reference 7.

molecular modeling suggests that these will show favorable electrostatic interactions.[7] In all of the solvents used, therefore, ^3J(H2,H3) indicates a mixture of folded-out and folded-in conformers. A weak NOE cross-peak in the ROESY spectrum is completely consistent with this analysis. **1** exhibits a much stronger H3−H11 cross-peak, indicating a higher portion of folded-in conformer. Unfortunately, even at elevated temperatures, the H4−H11 and H4−H6Me cross-peaks which are diagnostic of the folded-out conformational family were obscured by other signals; their presence can only be inferred. The H5−H6Me cross-peak, previously found to be diagnostic for both conformations,[7] was observed in the spectrum. Modeling calculations were in agreement with this interpretation. Both folded-out and folded-in conformational families of **3** were found, but the folded-out family was more densely populated. In the folded-in conformer, the torsional angle H2−C2−C3−H3 was approximately 100°. The simulated folded-in conformers showed a close proximity of H3 to H11 and H4 to H6Me, while the folded-out conformers showed contact between H4 and H11. All of the cross-peaks in the ROESY spectrum of **3** were satisfied by one or both conformational families. Figure 3 shows the superposition of the computer generated folded-out and folded-in conformers of **3** in DMSO together with the representative X-ray folded-in and folded-out conformations.

Table 3 shows the effect of temperature on ^3J(H2,H3) in DMSO-d_6 for **1**, **2**, and **3**. This is the only coupling constant to change significantly with temperature. **1** exhibits a steady increase in ^3J(H2,H3) values,[7] indicating an increase in the abundance of the folded-out conformers. By contrast, **2** shows an increase in the portion of folded-in conformers, as evidenced by the decrease in ^3J(H2,H3) (Table 3). For **3**, ^3J(H2,H3) is the same at all temperatures studied, at around 6.7 Hz. This is an intermediate value, suggesting that both folded-out and folded-in families are heavily populated. It may be that for all three compounds the energies of the folded-out and folded-in

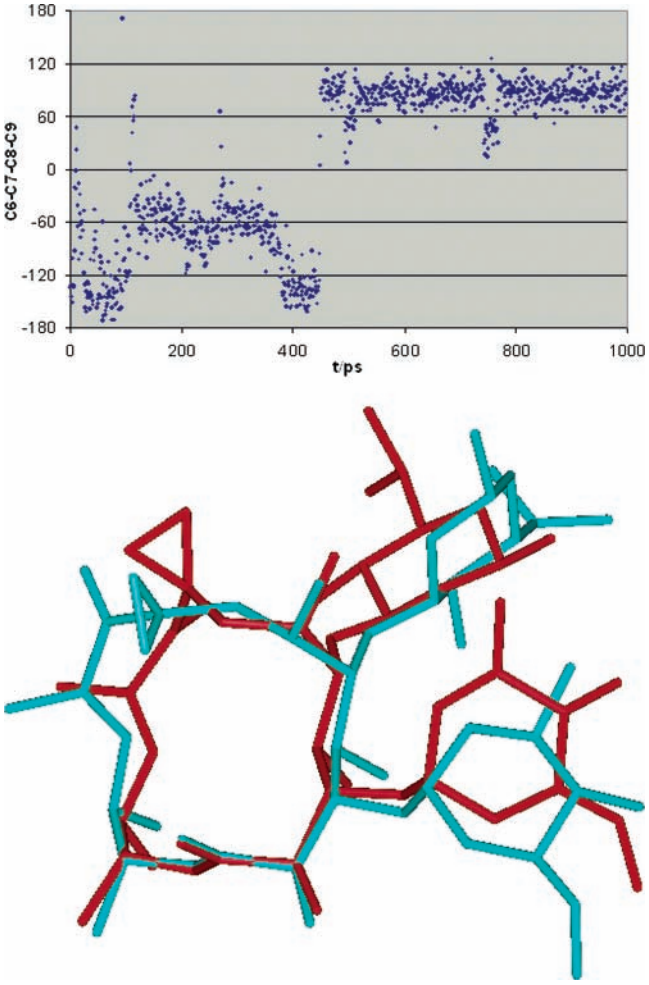

Figure 4. Torsion angle C6−C7−C8−C9 during MD simulation in $CDCl_3$ for compound **3** (top) and superposition of the averaged conformations of **3** representing the two different positions of the upper part of the lactone ring (bottom). The blue structure represents the conformations with a torsion angle of around −60°, while the red structure represents conformations with a torsion angle of around 100°.

conformations are very similar and all three converge toward equal population as the temperature rises.

Apart from the variations in the lower part of the lactone ring (which is described by C3−C5 folded-in and folded-out conformations), molecular modeling data presented evidence for conformational changes also in the C8−C11 region of the lactone ring not covered by NMR data due to the lack of proton−proton correlations.The torsion angle C6−C7−C8−C9 exhibited almost discrete changes (Figure 4) reflecting the twist of the epoxy ring from the plane of the lactone ring, which was more pronounced for **3** having the C10═C11 double bond. Results of the simulations excluded the possibility of the creation of a hydrogen bond between the oxime hydrogen and epoxy oxygen in **2**. A formation of this particular hydrogen bond might account for the observed conformational changes in the C8−C11 part of the lactone ring being more pronounced for compounds having a carbonyl instead of an oxime group at position 9. Since no hydrogen bond was indicated, the other possible reason for the increased rigidity of the compound with the oxime group would be the existence of the imino−enamino tautomerism. However, signals that would correspond to the enamino form were not observed in the NMR spectra neither at room temperature nor at the elevated temperatures (293−373 and 243−323 K in DMSO-d_6 and $CDCl_3$, respectively). Therefore, no evidence for imino−enamino equilibrium was found. According to modeling results, solvent influence on structural changes in the C8−C11 part of the lactone ring was found to be larger for **3**, having the double C10═C11 bond.

Conformations of the Desosamine and Oleandrose Sugars. The ROESY spectra of **1**−**3** show all of the expected cross-peaks for sugars in the Everett−Tyler chair conformation.[12] The large diaxial homonuclear coupling constants (e.g., ^3J(2′H,3′H) = 9.9 Hz) are also consistent with chair conformations (Table 2). Intersugar contacts H1′−H5″ suggest that the alpha faces of the two sugars are close (the up−up arrangement) and contacts such as H1′−H5, H1′−H4Me, H1″−H3, and H1″−H2Me define the relative position of the two sugars with respect to the macrocycle. The observed intrasugar cross-peaks characteristic for the desosamine chair conformation were H1′−H3′, H3′−H5′, H1′−H5′, and H2′−H4′a, and those for oleandrose were H2″a −H4″ and H4″−H5″Me. Molecular dynamics calculations reveal however that this arrangement of sugars may not be quite so stable as in erythromycin. The fluctuations in H1″−H3 and H1″−H2Me contacts were noticed, while they did not occur in H1′−H5 and H1′−H4Me contacts. Flexibility about the oleandrose glycosidic bond is therefore indicated. A higher rigidity of the desosamine sugar appears not to be affected by conformational changes in the oleandrose moiety. The relative positions of sugar rings with respect to the lactone ring in **2** and **3** were similar to those previously observed for **1** and its 8-methylene derivative;[7] that is, the oleandrose adopts dominantly a coplanar position, while desosamine is perpendicular with respect to the lactone ring.

Interactions with *E. coli* Ribosomes. The binding of ligands to target molecules can be studied by a variety of NMR methods, depending on the sizes of the compounds and the kinetics of binding. Current methodology has been reviewed.[27−29]

For this study, we adopted two methods. The trNOESY experiment was used to determine the conformations of the ligands in the bound state. We combine this with STD methodology. STD is a very sensitive method that allows the mapping of binding epitopes.[19] Saturation of a single target resonance can result in a rapid spread of saturation over the entire macromolecule if spin diffusion within the macromolecule is efficient. The ligand resonances also become saturated provided that the ligand protons are close in space to the macromolecular protons. The degree of saturation of the individual ligand resonances depends on the binding kinetics and the distance of the protons involved. The STD amplification factor (A_{STD}) can be used to quantify this information.

$$A_{STD} = \frac{I_o - I_{sat}}{I_o} = \frac{I_{STD}}{I_o} \quad (1)$$

where I_0 and I_{sat} are peak intensities in off-resonance (reference) and on-resonance spectra, respectively.

As a control experiment, we first recorded NMR spectra (trNOESY and STD) of azithromycin in contact with *E. coli* ribosomes for which the trNOESY experiments[16] as well as X-ray crystallography[3] confirmed that complexes were formed. The trNOE data obtained in our study for a solution of azithromycin and *E. coli* ribosomes were in good agreement with those previously observed.[16] The binding of azithromycin to the ribosome was identified by the negative sign, size, and buildup rate of the transferred NOEs. The analysis of trNOE data showed that free and bound conformations of azithromycin are similar, which is in agreement with X-ray data[3].

The STD experiment was initially performed on azithromycin, a drug for which crystallographic data are available. The STD

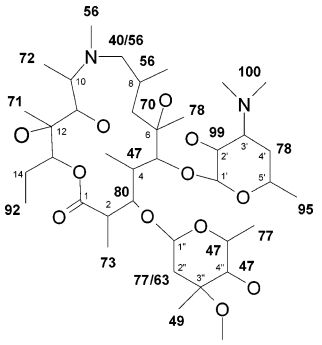

Figure 5. STD enhancements of azitromycin bound to *E. coli* ribosomes. The relative degrees of saturation (%) of the individual protons are normalized to H-6Me.

intensities of individual signals were measured relative to the corresponding signal intensities in the reference spectrum. The saturation produced the largest enhancement of the desosamine N−CH_3 groups and H2′ proton (Figure 5). Strong enhancements were observed for methyl groups at positions C5′ and C14 and the proton H3. Somewhat smaller enhancements of methyls at C2, C6, C10, and C12 were also observed (Figure 5). X-ray data[2,3] showed that the main interactions between macrolide antibiotics such as erythromycin, clarithromycin, or azithromycin and ribosomes involved hydrogen bonding between OH-2′ on the desosamine ring and OH-6, OH-11, and OH-12 on the lactone ring and adenine and uracil residues. The hydrophobic effect was also shown to play a significant role in the stabilization of the complex. The results obtained from STD NMR measurements of azithromycin generally correlate with crystallographic data, although a few small differences are observed such as a moderate STD enhancement of the macrocycle N−CH_3 protons and strong enhancements of methyl protons at position 15, for example (Figure 5). These may be due to the fact that NMR detects a preinhibition binding,[16−18] while X-ray crystallography measures a strong inhibitory effect.[2−4] Additionally, structural features of the complex may not be exactly the same in solution and in the solid state.[30] Also, the discrepancies found between crystal structures of complexes between macrolides and in particular azithromycin and ribosomes isolated from different species (*H. marismortui*[3] and *D. radiodurans*[2,4]) are still not completely understood, and therefore, solution state NMR measurements as described in this paper can help in further characterization of these interactions.

Subsequently, we recorded 1D STD NMR spectra of **1** (Figure 6) as well as **2** and **3** in the presence of *E. coli* ribosomes. Compared to azithromycin, STD signals were found to be significantly weaker in **1**−**3** which might be an indication of different exchange rates for these two classes of macrolides. For **1**, the saturation produced the largest enhancement of the H12 that was set to 100% and the relative degrees of saturation of other protons were normalized to that of H12. The protons H4 and H2′ were moderately enhanced, the former more strongly than the latter. Compound **2** exhibited stronger overall STD enhancements than **1** and **3**, especially in the upper left lactone region, for example, C10−C12 (Figure 7). The largest saturation transfer was observed for methyl protons at position 10. The closest proximity of this methyl group to the ribosome surface might be an indication that this part of the molecule is buried deeper into the ribosome ensemble by forming hydrogen bonding interactions involving oxime and/or hydroxyl groups at positions 9 and 11, respectively. The largest STD enhancements in **3** were observed at the desosamine sugar for the methyl group at position C5′ and the H6 proton of the lactone ring.

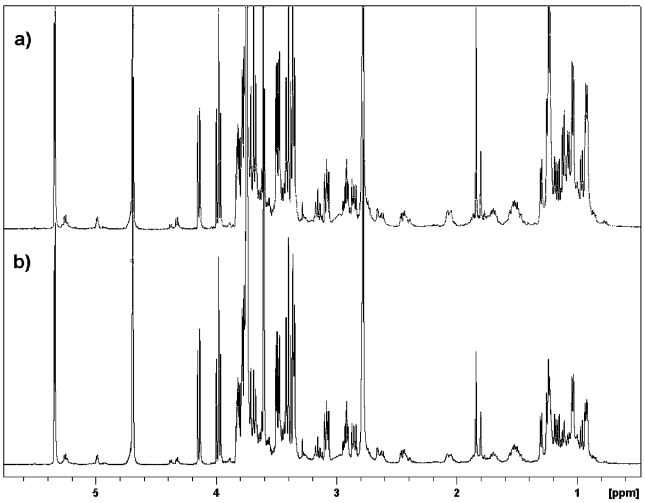

Figure 6. (a) Off-resonance (reference) and (b) on-resonance NMR spectra of oleandomycin in contact with *E. coli* ribosomes.

Unfortunately, protons H2′ in **2** and **3** were overlapped with signals of the Tris buffer and no STD effect could be unambiguously determined. Small enhancements were also observed for CH_3 protons at position 12. It is interesting to note that oleandrose did not exhibit appreciable STD enhancements, showing that this sugar is not likely to be involved in binding interactions, being consistent with X-ray data for cladinose sugar in the related 14-membered erythromycin and clarithromycin.[2] On the other hand, cladinose in 15-membered macrolide azithromycin showed STD enhancements (Figure 3) in agreement with crystal structures of *H. Marismortui* ribosomes complexed with azithromycin.[3]

Although different saturation transfers were observed for azithromycin and **1**−**3**, one can generally assign three main common parts of the macrolides in contact with ribosomes, that is, the desosamine sugar, the region C3−C6, and the region C10−C14, both at the lactone ring. The variations in STD enhancements can be attributed to structural differences of the studied molecules, especially in the upper lactone region, but also to different conformational properties and overall molecular shapes.

To deduce the binding conformations of **1**−**3**, we attempted trNOE experiments. Contrary to 15-membered macrolide azithromycin, trNOE effects were not observed for the solutions of **1**−**3** and deuterated *E. coli* ribosomes even with varying the ligand concentrations and lowering the temperatures. This may be due to unfavorable binding kinetics[28,30−32] of these 14-membered oleandomycin-like compounds. Namely, if the off rate for the ligand−ribosome complex is not appreciably greater than the NOE buildup rate in the complex, an efficient transfer of NOEs between bound and nonbound oleandomycins will not occur during the relatively short mixing times (here 100−200 ms) used in trNOE experiments. On the other hand, the saturation times employed in STD experiments in this study were more than 10 times higher (2−4 s), and this extra time for NOE buildup may allow the observation of STD effects (although weak) even if trNOEs are not observable.

A comparison of the observed STD NMR enhancements of **1**−**3** mapped onto the solution state structures, as shown in Figure 7 with STD enhancements found for azithromycin and structures of azithromycin−ribosome complexes available from X-ray data, reveals similarities and defines molecular surfaces of ligands in close contacts with the ribosomes. This information could be used to guide medicinal chemists in order to design

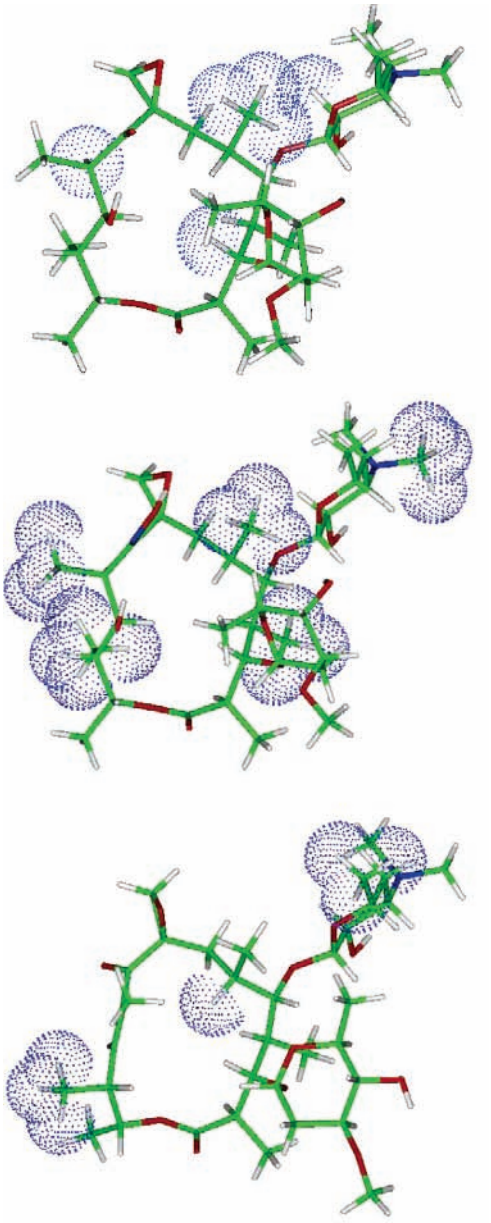

Figure 7. STD binding epitopes of **1**−**3** mapped onto the solution state structures as determined by molecular modeling and NMR.

higher affinity oleandomycins and to assist in overcoming the resistance problems. Once the key structural elements responsible for the activity are determined, one can also modify other parts in the molecule to optimize physicochemical properties, which dictate cellular and in vivo potency and efficacy as well as oral bioavailability. These include solubility and absorption, distribution, metabolism, excretion, and toxicity (ADMET), shown to be critical bottlenecks for macrolides to reach higher developmental phases.

Conclusions

This investigation has shown that oleandomycin derivative **2** adopts predominantly the folded-out conformation in the C3−C5 region of the macrocycle ring in solution, while for **3** a mixture of folded-in and folded-out conformations has been observed. It has been demonstrated that both the H2−H3 coupling constant and characteristic H3− H11 and H4− H11 NOE cross-peaks are good indicators of macrocycle conformational changes in solution. Desosamine and oleandrose are both found to exist in chair conformations, with the latter showing higher conformational flexibility around the glycosidic bond. Modeling calculations have indicated changes in the upper macrocyclic region in the studied compounds and discarded the possibility of forming intramolecular hydrogen bonds involving epoxy oxygen. The binding epitopes of **1**−**3** in interaction with *E. coli* ribosomes were determined by STD NMR spectroscopy. Three main structural parts of the studied macrolides have been identified to be in close contact with the ribosome, the desosamine sugar, and the two regions at the lactone ring, C3−C6 and C10−C14. This is consistent with available crystallographic data of the related ribosome−macrolide complexes. However, the observed variations in binding epitopes reflect structural and conformational differences and overall shape differences of the investigated molecules. Finally, a combined use of NMR spectroscopy and molecular modeling as described here has proven to be a valuable tool to determine conformational properties of oleandomycin-like compounds and to characterize their interactions with ribosome and together with available X-ray structures of related ribosome−macrolide complexes provide sound basis for design of the next-generation oleandomycins and macrolides in general.

Acknowledgment. We are indebted to Gordana Turkalj who kindly provided the samples. We thank Gorjana Lazarevski and Norber Müller for helpful comments and discussions.

Supporting Information Available: Two Protein Data Bank tables and one graphic showing STD enhancements for **1**−**3**. This material is available free of charge via the Internet at http://pubs.acs.org.

References and Notes

(1) Poehlsgaard, J.; Douthwaite, S. *Curr. Opin. Invest. Drugs* **2003**, *4*, 140.
(2) Schlünzen, F.; Zarivach, R.; Harms, J.; Bashan, A.; Tocilj, A.; Albrecht, R.; Yonath, A.; Franceschi, F. *Nature* **2001**, *413*, 814.
(3) Hansen, J. L.; Ippolito, J. A.; Ban, N.; Nissen, P.; Moore, P. B.; Steitz, T. A. *Mol. Cell* **2002**, *10*, 117.
(4) Berisio, R.; Harms, J.; Schlünzen, F.; Zarivach, R.; Hansen, H. A. S.; Fucini, P.; Yonath, A. *J. Bacteriol.* **2003**, *185*, 4276.
(5) Hochstein, F. A.; Els, H.; Celmer, W. D.; Shapiro, B. L.; Woodward, R. B. *J. Am. Chem. Soc.* **1960**, *82*, 3225.
(6) Lazarevski, G.; Kobrehel, G.; Dokić, S.; Kolačny-Babić, L.; Kojić-Prodić, B.; Janković, D.; Puntarec, V. *J. Antibiot.* **1994**, *47*, 349.
(7) Novak, P.; Banićc Tomišić, Z.; Tepeš, P.; Lazarevski, G.; Plavec, J.; Turkalj, G. *Org. Biomol. Chem.* **2005**, *3*, 39.
(8) Steinmetz, W. E.; Sparow, A.; Somsouk, M. *Magn. Reson. Chem.* **2005**, *43*, 16.
(9) Steinmetz, W. E.; Shapiro, B. L.; Roberts, J. J. *J. Med. Chem.* **2002**, *45*, 4899.
(10) Steinmetz, W. E.; Sadowsky, J. D.; Rice, J. S.; Roberts, J. J.; Bui, Y. K. *Magn. Reson. Chem.* **2001**, *39*, 163.
(11) Bertho, G.; Gharby-Benarous, J.; Ladam, P.; Delaforge, M.; Girault, J. P. *Bioorg. Med. Chem.* **1998**, *6*, 209.
(12) Everett, J. R.; Tyler, J. W. *J. Chem. Soc., Perkin. Trans. 2* **1987**, 1659.
(13) Lazarevski, G.; Vinković, M.; Kobrehel, G.; Dokićc S.; Metelko, B.; Vikić-Topić, D. *Tetrahedron* **1993**, *49*, 721.
(14) Awan, A.; Brennan, R. J.; Regan, A. C.; Barber, J. *J. Chem. Soc., Perkin Trans. 2* **2000**, 1645.
(15) Košutić-Hulita, N.; Matak-Vinković, D.; Vinković, M.; Novak, P.; Kobrehel, G.; Lazarevski, G. *Croat. Chem. Acta* **2001**, *74*, 327.
(16) Awan, A.; Brennan, R. J.; Regan, A. C.; Barber, J. *J. Chem. Soc., Chem. Commun.* **1995**, 1653.
(17) Bertho, G.; Ladam, P.; Gharby-Benarous, J.; Delaforge, M.; Girault, J. P. *Int. J. Biol. Macromol.* **1998**, *22*, 103.
(18) Evrard-Todeschi, N.; Gharby-Benarous, J.; Gaillet, C.; Verdier, L.; Bertho, G.; Lang, C.; Parent, A.; Girault, J. P. *Bioorg. Med. Chem.* **2000**, *8*, 1579.
(19) Mayer, M.; Meyer, B. *J. Am. Chem. Soc.* **2001**, *123*, 6108.
(20) Bax, A.; Davis, D. G. *J. Magn. Reson.* **1985**, *63*, 207.
(21) Bax, A.; Summers, S. F. *J. Am. Chem. Soc.* **1986**, *108*, 2093.
(22) Hwang, T.-L.; Shaka, A. K. *J. Am. Chem. Soc.* **1992**, *114*, 3157.
(23) Piotto, M.; Saudek, V.; Sklenar, V. *J. Biomol. NMR* **1992**, *2*, 661.

(24) Sklenar, V.; Piotto, M.; Leppik, R.; Saudek, V. *J. Magn. Reson., Ser. A* **1993**, *102*, 241.
(25) Allen, F. H. *Acta Crystallogr*. **2002**, *B58*, 380.
(26) Ogura, H.; Furuhata, K.; Harada, Y.; Iitaka, Y. *J. Am. Chem. Soc.* **1978**, *100*, 6733.
(27) Peng, J. W.; Moore, J.; Abdul-Manan, N. *Prog. NMR Spectrosc*. **2004**, *44*, 225.
(28) Meyer, B.; Peters, T. *Angew. Chem., Int. Ed*. **2003**, *42*, 864.
(29) Stockman, B.; Dalvit, C. *Prog. NMR Spectrosc.* **2002**, *41*, 187.
(30) Johnson, M. A.; Pinto, B. M. *Bioorg. Med. Chem*. **2004**, *12*, 295.
(31) Clore, G. M.; Gronenborn, A. M. *J. Magn. Reson.* **1983**, *53*, 423.
(32) Clore, G. M.; Gronenborn, A. M. *J. Magn. Reson.* **1982**, *48*, 402.